

Subtype Selectivity of Dopamine Receptor Ligands: Insights from Structure and Ligand-Based Methods

Qi Wang,[†] Robert H. Mach,[†] Robert R. Luedtke,[‡] and David E. Reichert*,[†]

Division of Radiological Sciences, Mallinckrodt Institute of Radiology, Washington University School of Medicine, 510 South Kingshighway Boulevard, St. Louis, Missouri 63110, and Department of Pharmacology and Neuroscience, University of North Texas Health Science Center, Fort Worth, Texas, 76116

Received July 15, 2010

Subtype selective dopamine receptor ligands have long been sought after as therapeutic and/or imaging agents for the treatment and monitoring of neurologic disorders. We report herein on a combined structure-and ligand-based approach to explore the molecular mechanism of the subtype selectivity for a large class of D₂-like dopamine receptor ligands (163 ligands in total). Homology models were built for both human D_{2L} and D₃ receptors in complex with haloperidol. Other ligands, which included multiple examples of substituted phenylpiperazines, were aligned against the binding conformations of haloperidol, and three-dimensional quantitative structure activity relationship (3D-QSAR) analyses were carried out. The receptor models show that although D₂ and D₃ share highly similar folds and 3D conformations, the slight sequence differences at their extracellular loop regions result in the binding cavity in D₂ being comparably shallower than in D₃, which may explain why some larger ligands bind with greater affinity at D₃ compared to D₂ receptors. The QSAR models show excellent correlation and high predictive power even when evaluated by the most stringent criteria. They confirm that the origins of subtype selectivity for the ligands arise primarily due to differences in the contours of the two binding sites. The predictive models suggest that while both steric and electrostatic interactions contribute to the compounds' binding affinity, the major contribution arises from hydrophobic interactions, with hydrogen bonding conferring binding specificity. The current work provides clues for the development of more subtype selective dopamine receptor ligands. Furthermore, it demonstrates the possibility of being able to apply similar modeling methods to other subtypes or classes of receptors to study GPCR receptor–ligand interactions at a molecular level.

INTRODUCTION

Dopamine receptors are members of a large class of G-protein coupled receptors (GPCRs) for biogenic amines which are essential for the normal activities of vertebrate central nervous systems (CNS). Dopaminergic neurotransmission is mediated by five receptor subtypes (D₁–D₅) in the CNS. Dysfunction of the cerebral dopaminergic system has been implicated in a variety of neurological and neuropsychiatric disorders, such as schizophrenia, Parkinson's disease, and drug addiction.¹ Since it has been found that different subtype receptors play distinct pathological roles in the G-protein signaling pathways of these disorders, subtype selective ligands are desired for the development of CNS drugs and/or imaging agents for the treatment or diagnosis of neurological and neuropsychiatric diseases.²

Among the five subtypes of dopamine receptors that have been characterized, the D₂, D₃, and D₄ receptors are classified as members of the D₂-like family. There are two isoforms for D₂ receptors: D_{2S} (short) and D_{2L} (long). D₂ and D₃ receptors share the greatest homology among the D₂-like family, with more than 50% amino acid sequence identity overall, and 79% homology within the transmembrane (TM)

domains.³ However, in the pursuit of pharmacotherapeutic agents with reduced side effects, or receptor subtype specific imaging agents, it would be desirable to have D₂/D₃ selective ligands because of their different pharmacological properties and neuroanatomical locations in the brain. The development of D₂ and D₃ receptor selective ligands has been a major research effort in many laboratories and has resulted in the development of moderately selective ligands over the past few years.^{4–14} To further improve the selectivity of these lead compounds, structure–activity relationships have been studied using computational drug design approaches. However, the majority of work has focused on maximizing the selectivity for D₂/D₄ or D₃/D₄ subtypes, since D₄ is more phylogenetically distant. So far, the most D₂/D₃ selective ligands are about 100-fold more selective, and only one QSAR study examining this selectivity has been reported. Salama et al. reported on QSAR studies using a data set of 79 D₂/D₃ receptor ligands, correlating their selectivity with 3D descriptors using CoMFA/CoMSIA approaches.¹⁴ The challenge to designing D₂/D₃ selective ligands is increased by the lack of X-ray diffraction structural data about the dopaminergic or even any aminergic receptors. As a result, the origin for the selectivity of the ligands remains elusive at a structural molecular level.

The recently reported crystal structure of the human β₂-adrenergic receptor^{15–17} opens a new channel for the rational design of more subtype selective dopamine receptor ligands

* To whom correspondence should be addressed. Phone: (314) 362-8461. Fax: (314) 362-9940. E-mail: reichert@wustl.edu.

[†] Washington University School of Medicine.

[‡] University of North Texas Health Science Center.

from a structure-based perspective. The β_2 -adrenergic receptor is more homologous to the dopamine receptors than bovine rhodopsin,^{18–20} which had previously been the sole available structure template for homology modeling of GPCRs. The comparison between bovine rhodopsin and the β_2 -adrenergic receptor revealed important structural differences between rhodopsin and other class A GPCRs, particularly in the (a) orientation and positions of the TM regions and (b) structure of the loop regions,^{15,21,22} which are important for the ligand (agonist/antagonist) binding and activation of the receptors. Compared to bovine rhodopsin, the crystal structure of the β_2 -adrenergic receptor provides a better template for homology modeling of dopamine receptors, because of its higher sequence identity/similarity to the latter, especially in the loops. Moreover, the structure of the β_2 -adrenergic receptor contains a diffusible ligand carazolol, which is a partial inverse agonist, in contrast to the covalently bound ligand retinal in rhodopsin. This makes it a notable template to study receptor–ligand interactions. Using the β_2 -adrenergic receptor as the template, several models of the dopamine receptors have been reported using different homology modeling approaches,^{13,23,24} and receptor–ligand interactions were evaluated at the molecular level for some ligands.

In this work, we report a combined structure- and ligand-based method to further explore the molecular mechanism of ligand selectivity for D₂/D₃ receptors. Homology models were built for both receptors complexed with haloperidol, using the crystal structures of both the β_2 -adrenergic receptor and bovine rhodopsin as templates. Molecular dynamics simulations were performed to refine the models in explicit lipid bilayer/solvent environments. The conformations of haloperidol taken from the refined models were then used as templates to align a library of 162 compounds for further 3D-QSAR analyses. Predictive models were established by CoMSIA methods for both D₂ and D₃ receptors correlating the ligands' affinities (K_i values). Overlay of the two receptor structures, along with the alignments of the whole ligand library at their active sites, reveals several novel structural features of the receptor subtypes, shedding light on the origins of ligand selectivity for D₂/D₃ receptors at the molecular level.

MATERIALS AND METHODS

Homology Modeling of D₂/D₃ Receptors. The homology models of D₂ or D₃ receptors were obtained by comparative modeling in the program MODELLER9.2,²⁵ using the crystal structure of the human β_2 -adrenergic GPCR (PDB code: 2RH1)¹⁵ and the bovine rhodopsin (PDB code: 1F88)¹⁸ as the templates. The sequence alignments were obtained by the automated sequence alignment program ClustalW²⁶ with some manual adjustments in the loop regions to maximize homology. There are significant sequence diversities in the loop regions for the D₂/D₃ receptors, as well as for the templates, especially at the intracellular loop region 3 (IL3). For the crystal structure of β_2 -adrenergic receptor (PDB code: 2RH1), this region was replaced by T4 lysozyme to increase the solubility and stability of the receptor; while for rhodopsin, this loop is much shorter. Since the active site of the GPCRs is located in the extracellular region near loop2 (EL2), the IL3 loop is unlikely to play a major role in ligand

binding. In order to improve the quality of the MODELER results, it was removed from the modeling process for both of the targets. For EL2, the sequences of both D₂ and D₃ receptors are much shorter (total length only about 10 residues) than either the human β_2 -adrenergic receptor or bovine rhodopsin and likely play a critical role in forming the binding site for small molecular ligands.²⁷ A conserved disulfide bond was built between EL2 and TM3 to rigidify the structure. Loop refining was automated by using the “very fast” refinement method within MODELER. A total of 50 models per receptor subtype were obtained. The model with the lowest DOPE energy calculated by MODELER was then picked and exported to SYBYL7.2²⁸ for further manipulation.

In SYBYL, the bound ligand was modified manually to the D₂/D₃ antagonist, haloperidol. Hydrogen atoms were added to both the receptor and the ligand, treating the ligand as protonated. The structures were then minimized using the AMBER99 force field and the Gasteiger–Huckel partial charges for the ligand, with the protein backbone atoms fixed in position, to a gradient of 0.05 kcal/(mol·Å).

Model Refinement. The resulting model of haloperidol-bound D₂ or D₃ receptor was further refined by multiple molecular dynamics (MD) simulations²⁹ in explicit membrane/solvent environments. A POPC lipid bilayer membrane patch (75 Å × 75 Å) was generated in VMD1.8.6.³⁰ The protein was inserted into and combined with the membrane so that the lipid and water molecules overlapping with the protein were deleted. A 5 Å layer of TIP3P water molecules was added in the directions above and below the membrane, with exclusion radii of 3.3 Å to solvate the whole system. Counterions were also added to produce a salt concentration of 100 mM. All of the above manipulations were accomplished in VMD1.8.6.

The MD simulations were performed using the NAMD2.6 program³¹ with the all-atom CHARMM27 force field^{32,33} following a published protocol.³⁴ Specifically, for each receptor, a total of 10 copies of the system were prepared from the initial starting geometry. While each copy started with the same starting geometry, different sampling paths were initiated by different seed numbers; the use of multiple copies allows for better sampling of the system. For each simulation copy, the following five rounds of equilibrations were completed: (i) 2000 steps of energy minimization for the nonbackbone atoms; (ii) five cycles of a 500-step energy minimization with decreasing position restraints (1, 0.8, 0.6, 0.4, 0.2) on the protein Cα atoms; (iii) a gradual increase in the temperature from 50 K to 310 K in 100 000 steps (100 ps) of constant volume (NVT ensemble) simulation with restraints (with a force constant of 3 kcal/(mol·Å²)) applied to the protein Cα atoms; (iv) five 40 000 step (40 ps each, 200 ps in total) constant surface area ensemble MD equilibrations with decreasing positional restraints on the Cα atoms; and (v) 200 000 step (200 ps) equilibration without any restraints. A total of 500 ps/copy were run for the equilibration steps. Another 1500 ps simulation/copy were run for the production step, with the last 500 ps trajectory being collected and used for averaging the structure.

For each simulation copy, the time-averaged structure of the production run was obtained by removing water, lipids, and ions from the structure and retaining only the protein and the bound ligand, aligning each frame (1000 frames for a 500 ps trajectory) to the first one and averaging the

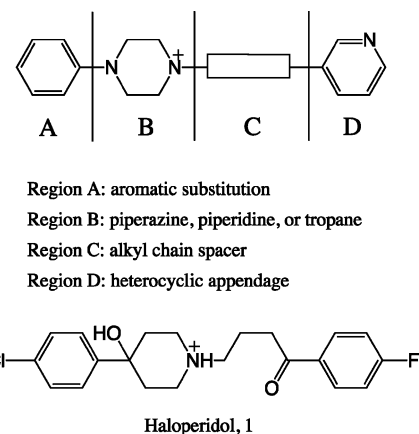


Figure 1. Structure of the previously reported D_2/D_3 ligands. Haloperidol is shown as the model ligand.

coordinates. The final averaged structure was obtained by aligning nine different time-averaged structures from different copies of simulations to the first one and averaging the coordinates. This structure was then minimized by 500 steps to remove any short-range repulsions. The minimized model was saved as the MD-refined, haloperidol-bound homology model of the D_2 or D_3 receptor and used for the subsequent studies.

In the simulations, a cutoff of 12 Å was used for nonbonded interactions, and long-range electrostatic interactions were treated using the Particle Mesh Ewald (PME) method.³⁵ Langevin dynamics and a Langevin piston algorithm were used to maintain the temperature at 310 K and a pressure of 1 atm. The r-RESPA multiple time step method³⁶ was employed with a 1 fs time step for bonded atoms, a 2 fs step for short-range nonbonded atoms, and a 4 fs step for long-range electrostatic forces. The bonds between hydrogen and heavy atoms were constrained with the SHAKE algorithm.

Ligand Alignments. Besides haloperidol, the ligands investigated in this study included 162 compounds synthesized earlier by (a) Mach and co-workers and (b) the Newman group at the National Institute of Drug Abuse (NIDA-IRP).^{4–9} All ligands were evaluated for affinity on human D_2/D_3 receptors using competitive radioligand binding protocols with the radioligand ^{125}I -IABN,^{4,5,37} thus ensuring consistency and comparability. The essential features of the scaffold include (a) a protonated nitrogen on a nonaromatic cyclic ring (piperazine, piperidine, or tropane; region B), (b) a heterocyclic appendage (region D) attached to the basic nitrogen by a spacer (region C), and (c) an aromatic substituent (region A) on position 4 of the piperazine/piperidine/tropane ring (Figure 1). The structure of the representative ligand, haloperidol, is shown in Figure 1. The structures for all of the compounds studied and their experimental K_i values are listed in the Supporting Information (Table 1).

The time-averaged haloperidol conformations from the MD-refined receptor complexes were separated from the models and manually modified into a starting 3D conformation for each ligand in SYBYL. The starting conformations were then imported into Maestro 5.1³⁸ and a conformer library for each ligand generated using the MCMM method found in MacroModel. ROCS 2.3.1³⁹ was used subsequently to retrieve the conformer from each library with the maximum shape alignment against the haloperidol reference

structure. All of the parameters were set to their default values. The program EON 2.0.1⁴⁰ was also employed to improve electrostatic overlap on the alignments by ROCS when necessary. This procedure was applied to obtain two different sets of ligand alignments for both the D_2 and D_3 binding sites, for the 3D-QSAR analysis described below.

3D-QSAR Analyses. The data set consisting of the aligned conformations of the 162 ligands plus haloperidol (163 compounds total) was then divided into training ($n = 122$) and test ($n = 41$) sets for 3D-QSAR study. Since the experimental D_2 and D_3 activities varied significantly, different training/test sets were built for the two cases. For D_2 , the 41 ligands forming the test set were **6, 14, 17, 22, 23, 29, 31, 40, 43, 46, 50, 59, 62, 67, 68, 70, 73, 76, 82, 85, 86, 88, 90, 93, 95, 97, 103, 107, 109, 114, 117, 120, 126, 131, 137, 141, 142, 146, 154, 159, and 161**. They were selected in such a way that their K_i values were randomly but uniformly distributed in the range of the values for the whole set so that the model's predictive power could be effectively evaluated.

For D_3 , the 41 ligands forming the test set were **2, 3, 4, 8, 20, 21, 25, 33, 39, 55, 58, 64, 68, 69, 72, 75, 76, 77, 80, 81, 89, 91, 92, 93, 96, 97, 99, 100, 101, 109, 113, 119, 123, 131, 133, 143, 148, 149, 154, 159, and 163**. The Gasteiger–Huckel partial charges were calculated for each ligand and used in the analyses. Several CoMSIA models were developed for the training set within the QSAR module of SYBYL using the default settings. The QSAR equations were calculated using the partial least-squares (PLS) algorithm. The cross-validated correlation coefficients R^2 (commonly referred to as q^2) were obtained by the leave-one-out (LOO) cross-validation technique. No column filtering was applied in any of the analyses. The predictive correlation coefficient (r_{test}^2) was determined by the predicted pK_i versus the experimental observed values in the test set.

In order to thoroughly evaluate the models' quality, a set of more rigorous criteria was used as suggested by Tropsha et al.^{41–43} For a predictive model tested in the test set, beside the r_{test}^2 , the coefficient of determination⁴⁴ and slope of regression lines when forcing the intercept through the origin are also needed to assess how far the predicted values deviated from the observed activities in the absolute scale. For a set of data (x_i, y_i) , the coefficient of determination R_0^2 was calculated as the correlation coefficient R^2 for a linear regression with the Y intercept set to 0.0 (i.e., described by $Y = KX$), which is different from the conventional R^2 for $Y = KX + b$. This test was incorporated because when actual vs predicted activities were compared, an exact fit was required instead of just a linear correlation. An intercept would imply additional adjustment for the prediction, thus higher inaccuracy.

Coefficients of determination were calculated as R_0^2 for predicted versus observed activities, and R'_0^2 for observed versus predicted activities. Slopes of regression lines, when forcing the intercept through the origin, were also calculated as K for predicted versus observed activities, and K' for observed versus predicted activities. These statistical parameters were then compared with the recommended values to assess the QSAR models.^{42,43}

Table 1. Selected Ligands and Experimental Binding Affinities (K_i) of the 163 Ligands Used in This Study^a

Ligand	Chemical Structure	D2 (nM)	D3 (nM)
1 haloperidol		1.1	13
9		5.5	580
11		101	150
22		21.5	0.2
32		24.1	1
35		0.05	0.3
46		1060	5.21
61		196	224
90		69	2.9
121		58.8	724

^a All values represent the average of multiple determinations as reported in the literature.^{4–9} (See Supporting Information Table 1 for a complete listing of all 163.) The compound number refers to the compounds as they are listed in the Supporting Information Table of all 162 compound that were used for this evaluation. The K_i values (nM) were determined using competitive radioligand binding protocols. Human D2L or D3 receptors expressed in stably transfected HEK-293 cells and the radioligand ^{125}I -IABN were used for these binding studies. The concentration of ^{125}I -IABN that was used was approximately equal to the K_d values for D2 (0.04 nM) and D3 (0.03 nM) dopamine receptors, and the compounds were evaluated over a 5 orders of magnitude dose range in triplicate using two concentrations per decade. IC50 values for the competition curves were determined using the computer program TABLECURVE. IC50 values were converted to K_i values. The K_i values shown represent the mean values for $n \geq 3$ determinations.

Table 2. The Distribution (in percentage) of the Backbone Dihedral Angles on Ramachandran's Plot for the Receptor Models before and after MD Refinements

model	% distribution			
	core	allowed	generous	disallowed
D ₂ (before)	85.0	13.0	1.2	0.8
D ₂ (after)	92.5	5.1	2.0	0.4
D ₃ (before)	84.5	11.2	2.8	1.6
D ₃ (after)	94.0	4.4	1.6	0.0

RESULTS AND DISCUSSION

Receptor Modeling. The initial structural homology models obtained with MODELER were then extensively refined with MD simulations, using their native environment of a fully solvated lipid bilayer. The simulations were run for a total of 20 ns (10 copies with 2 ns each), which resulted in extensive sampling of the protein conformation in its native environment. The ligand haloperidol was also included in the receptor modeling for the following reasons:

- (1) We are particularly interested in the ligand-bound conformation of the receptors, i.e., to exploit the receptor structure to guide the design of more selective and potent ligands. Therefore, we chose to build the ligand *in situ* to avoid a docking procedure. MD simulations were employed to effectively sample the conformational flexibility of both the receptor and ligand in the context of each other.
- (2) Haloperidol is a well characterized potent dopamine receptor antagonist. It binds to the D₂ and D₃ receptors relatively nonselectively (1.1 nM versus 13 nM). An antagonist in complex with the dopamine receptors provides a prototype to study receptor–ligand interactions. The use of an antagonist is important for consistency with the experimental methods used to measure the binding affinities; the assays are run under conditions ensuring that the receptor is in an inactive state.
- (3) Haloperidol is of intermediate size in the large compound library that was studied. The published D₂/D₃ compounds

consist of different sizes and lengths, with molecular weights ranging from 291 to 589 g/mol and volumes ranging from 922 to 1464 Å³ (calculated in SYBYL). For the convenience of ligand alignment, an intermediate-sized ligand would be a good template upon which to overlay other ligands. Haloperidol is also intermediate in the number of rotatable bonds (six) and by extension flexibility within the binding site, making it, as with molecular size, a good template for overlaying the other compounds.

To validate the MD-refined models, the stereochemical quality of the structures was evaluated using PROCHECK.⁴⁵ A comparison of the initial PROCHECK results and those after MD refinement showed that the models' stereochemical quality was greatly improved by the MD simulations (Table 2). For both the D₂ and D₃ receptors, >90% of the backbone dihedral angles now reside in the core regions, in contrast to 80% before refinement. Only one residue in the refined D₂ structure now falls in the disallowed regions of the Ramachandran plot.⁴⁶ It is actually located at the truncated cytoplasmic end of TM6, near the truncated loop IL3, distal from the orthosteric binding site. This deviation was, therefore, left unchanged.

The important role of EL2 has been emphasized for ligand binding of class A GPCRs,^{15,20,47} its modeling is, therefore, a critical component for a reliable receptor structure. The sequence length for EL2 varies widely within the class A GPCRs, which makes it a challenging task to successfully develop a homology model. In one recent work, the EL2 of dopamine receptors was modeled by modifying the sequence of it in the human β2-adrenergic receptor into the dopamine receptors, using a loop database and refined by MD simulations (*in vacuo*).¹³ In other models of dopamine receptors, the refinements were performed in a similar manner,^{23,24} focusing on the EL2 regions alone without a thorough sampling of the surrounding residues, especially the TM regions.

The MD-refined haloperidol bound D₂/D₃ receptor structures are shown in Figure 2. Compared with the structure

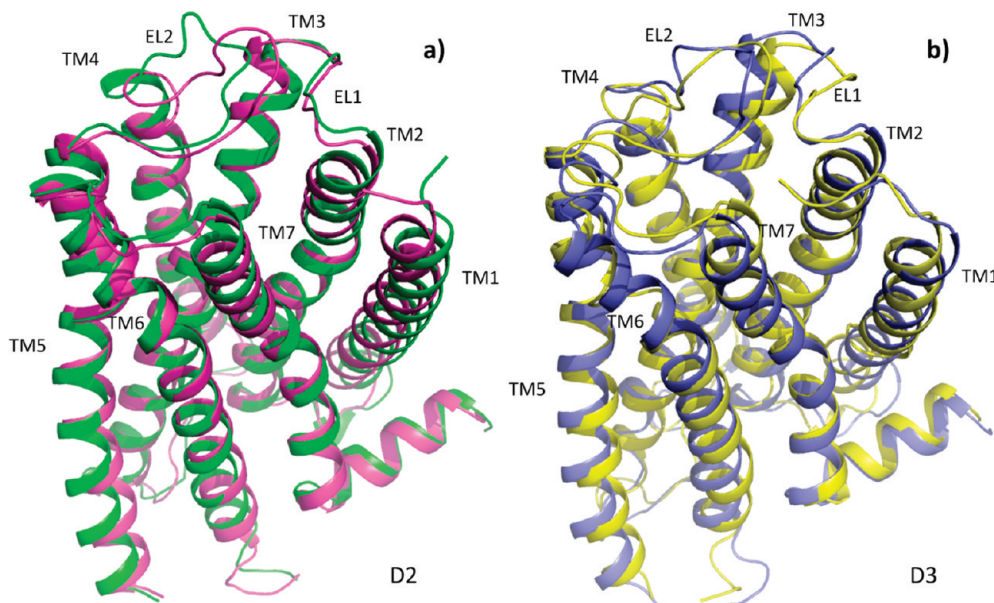


Figure 2. The models of D₂/D₃ receptors before and after MD refinements shown in cartoon representation. The TM regions and EL1 and 2 are labeled. (a) D₂ receptor before (magenta) and after (green) refinements. (b) D₃ receptor before (yellow) and after (blue) refinements.

before refinement, there are considerably large structure rearrangements for the receptor, especially in the loop regions, for both D₂ and D₃. A major characteristic movement, pertinent to ligand binding, is the retraction of EL2 away from EL1. The N-terminal part of EL2, which is more hydrophilic than the C-terminal part (D₂, NNADQNE; D₃, TTGDPT), lifts upward to interact with the extracellular solvents, while the C-terminal portion of EL2 goes into the binding site, making a hydrophobic contour capable of interacting with the ligand. The conserved disulfide linkage between TM3 and EL2 restricts the position of EL2.

Another observation is the rearrangement of the ligand at the orthosteric site (Figure 3). In D₂, some minor adjustments of the ligand are observed. The *para*-fluoro phenyl end of haloperidol tilts toward TM7 from the TM2/7 cleft, making a bend from its previous linear binding conformation. In contrast, in D₃, there is penetration of the *para*-chlorophenyl ring of the ligand deeper into the binding pocket. Examination of the D₂ counterpart reveals that a cysteine residue (C^{3,36}) resides in this location, making the ligand penetration impossible in D₂. Although D₂ and D₃ share an almost identical sequence for TM3, the adjacent EL1 for D₃ is one residue shorter than that for D₂ (D₂, GGVWNFS; D₃, GEWKFS). As a consequence, the TM3 helix of D₃ twists toward the extracellular end compared to D₂, forcing the same residue C^{3,36} in D₃ to shift away from the binding pocket, creating an empty space for the ligand to occupy (Figure 4). An estimation of the volume of the binding site⁴⁸ indicates that the binding site is 30–50% larger in D₃ than in D₂. The binding crevice is, therefore, more accessible to the extracellular aqueous solvent at D₂. The ligand selectivity for the two subtype receptors could partially result from a difference in the sizes of the two binding pockets. Our models suggest that, although D₂ and D₃ share a very high sequence identity in the TM regions, which make up most of the binding sites, different compositions of the loop regions could affect the contour and topography of the binding pockets, leading to binding selectivity. This effect was not unprecedented. In a comparison of the β_1 and β_2 adrenergic receptor crystal structures, it was observed that differences at distant receptor sites could confer subtype selectivity by influencing the conserved residues' conformations, kinetics, and dynamics.^{17,49}

Receptor–Ligand Interactions. Figure 5 shows the ligand haloperidol binding at the orthosteric site making extensive interactions with the receptors. The prominent salt bridge between the highly conserved Asp^{3,32} of the receptor and the protonated nitrogen on the piperidine scaffold of the ligand is responsible for the anchorage of the ligand. The ligand orientation is an L shape in D₂, with the *para*-chlorophenyl ring tilting toward TM4 and the *para*-fluorophenyl moiety bending toward TM7. The *para*-chlorophenyl ring is tightly flanked by residues of the aromatic clusters (W^{6,48}, F^{6,51}, F^{6,52}, and H^{6,55}) on TM6, the hydrophobic core (V^{3,33} and C^{3,36}) of TM3, and the hydrophobic residues (I183 and I184) on EL2. In addition to the salt bridge, there is a hydrogen bond between the hydroxyl substituent on the piperidinium ring of haloperidol and the side chain of Y^{7,35} on D₂. Besides that, S^{5,42} and S^{5,46} are also within close proximity of the *para*-chlorophenyl ring. Therefore, if there is a donor/acceptor substituent on the ring, it could also contribute to binding selectivity by hydrogen bonding with the serine residues deep within the pocket. At the other end

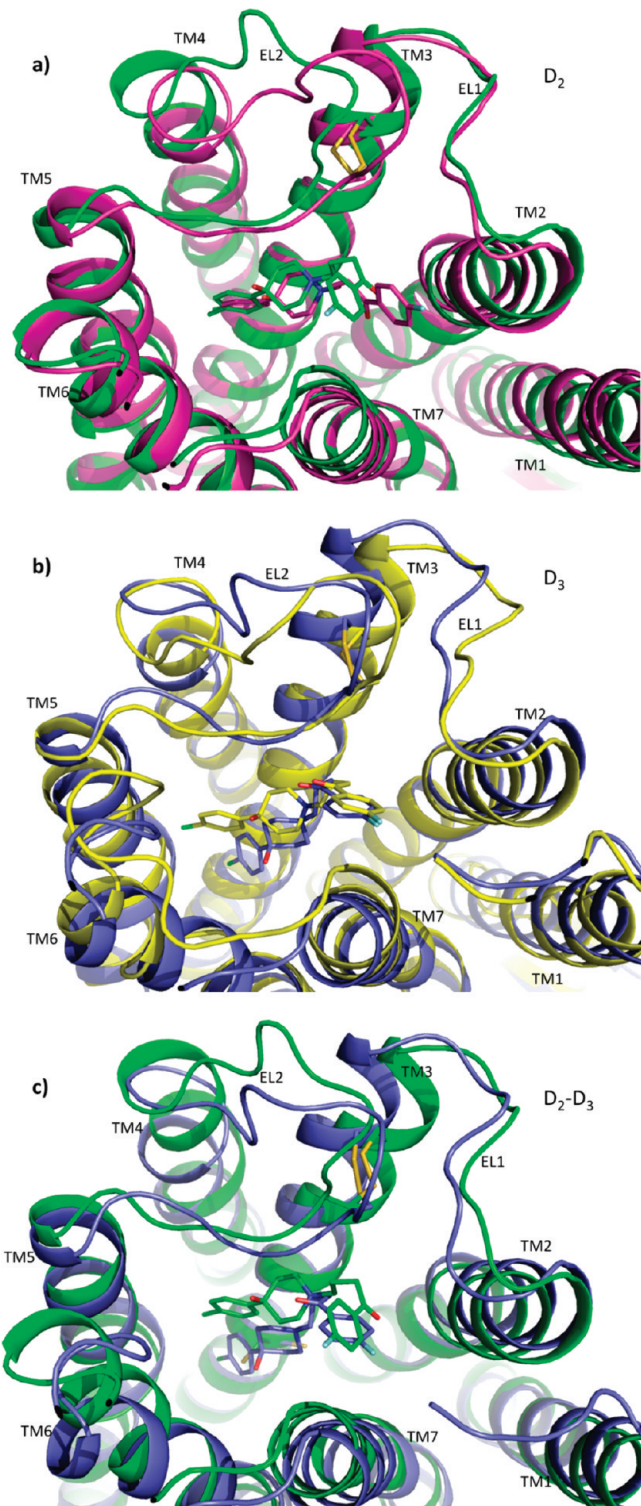


Figure 3. Close-up view of the orthosteric sites before and after refinements for D₂ and D₃. Haloperidol is shown as a stick model. (a) D₂ receptor before (magenta) and after (green) refinements. (b) D₃ receptor before (yellow) and after (blue) refinements. (c) D₃ overlaid with D₂.

of the ligand, the *para*-fluorophenyl moiety is relatively flexible, extending to the open cleft between TM2 and TM7. In contrast, for the D₃ receptor, the orientation of the ligand is almost linearly parallel with the axis of TM3, with a slight rotation of the *para*-fluorophenyl plane along the TM2 axis. The hydrophobic binding contour for the D₃ receptor consists of W^{6,48}, F^{6,51}, F^{6,52}, and H^{6,55} on TM6; V^{3,33}, C^{3,36}, and I^{3,40}

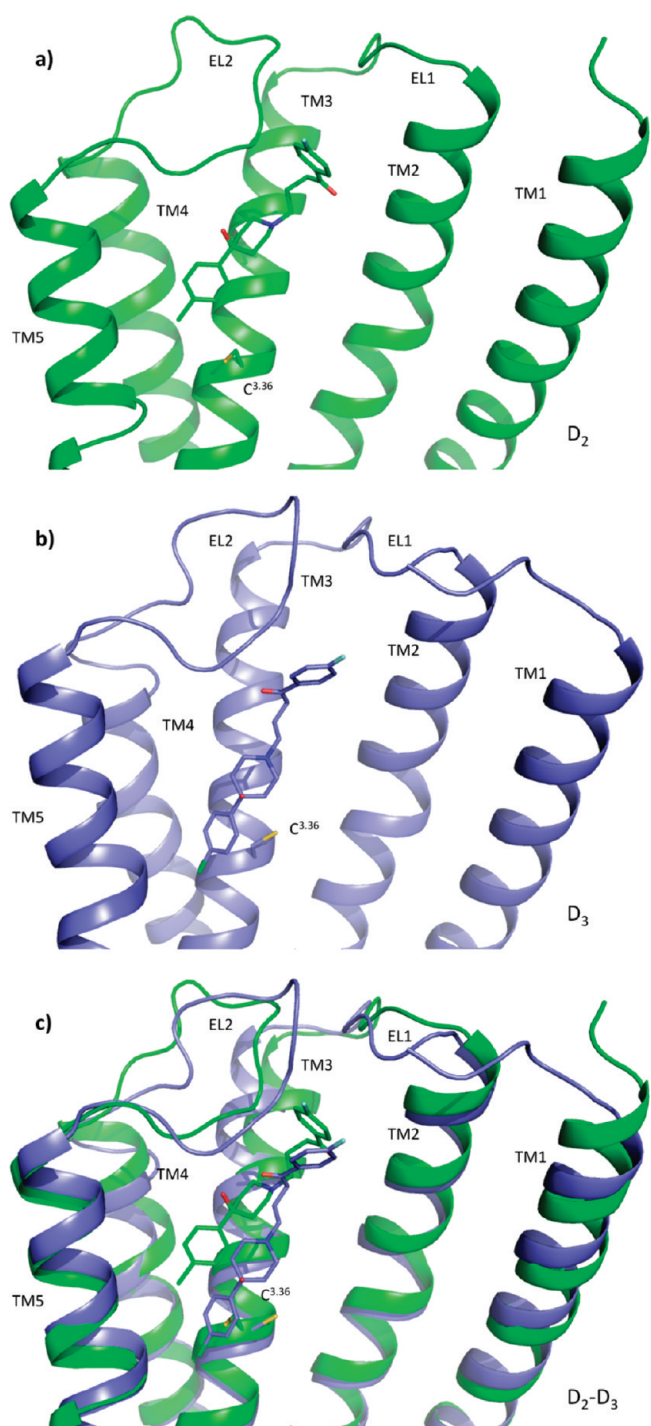


Figure 4. A comparison of the binding sites in D₂ and D₃. For clarity, TM6 and TM7 are removed. Haloperidol and the C^{3.36} residue are shown as stick models. (a) D₂; (b) D₃; (c) D₃ overlaid with D₂.

of TM3; and I183 on EL2. The binding site on D₃ looks like a tunnel, with the ligand fitting inside in a rod-like orientation. The ligands with longer spacer chains are better accommodated in the D₃ than in the D₂ binding site. Since the ligand is buried deeper, no hydrogen bond can be established between the hydroxyl group and any residue on D₃. Although Y^{7.35} is a conserved residue, it is too far away to establish a hydrogen bond with the hydroxyl group on haloperidol. The S^{5.42} and S^{5.46} residues, especially S^{5.42}, are also out of hydrogen bonding range. The importance of the hydroxyl substituent on the ligand as well as Y^{7.35} on D₂ for

their binding has been reported before^{7,50,51} and is confirmed in our receptor model. No other specific interaction is present between the ligand and receptor residues for both receptors. However, the binding pocket is delineated by the hydrophobic residues of TM2/3/6/7 and EL2, which could confer ligand selectivity by creating subtle differences in the binding site topography.

The analysis of receptor–ligand interactions confirms that most residues at the binding site are conserved, yet structurally (3-dimensionally) dissimilar between the D₂ and D₃ receptors. Consequently, using the receptor models to design ligands with greater ligand selectivity remains a challenging task. However, our comparative modeling studies suggest that consideration of the overall binding site contours, instead of individual residues on the receptors, will be required to further optimize the lead compounds for binding selectivity.

Ligand Alignments. Establishing a suitable alignment is the most crucial step to successfully building a 3D-QSAR model, especially for a large set of structurally diverse ligands. In our work, the ligand alignments were achieved by using the ROCS program to overlay a conformer library for each ligand upon the bound conformation of haloperidol, retrieving the conformation with the maximum pharmacophore overlap with the query (haloperidol), based on matching both 3D shape and chemistry. A good superposition of the conserved protonated amine of all the ligands over that of haloperidol was used as a prerequisite to establish the alignments. Since ROCS only uses the heavy atoms of a ligand, the protons on the amines were not taken into consideration for shape superimposition. EON was also used to refine the ROCS hits by electrostatic similarity. Nevertheless, sometimes the output still returned the top scoring hit with a mismatched H atom at the amine terminal. In this case, the nitrogen center was manually inverted, and another round of conformer generation-ROCS alignment-EON refinement was carried out. This iteration process was repeated multiple times until a satisfactory alignment (visual inspection) was achieved for the particular ligand. For a ligand L1 with large structural deviation from haloperidol, a straightforwardly precise superimposition with haloperidol could be difficult to obtain or determine. To deal with this situation, a second ligand, L2, which is more similar to the target ligand L1, but previously aligned with haloperidol, was then used as the query structure instead to obtain the alignment for the target (L1).

The superimposition for all 163 ligands is depicted in Figure 6a and b, respectively, along with the orthosteric sites of the MD refined D₂ and D₃ receptor models. As the primary recognition element, the central moiety, which could be piperazinium, piperidinium, or tropanium, is responsible for securing the overall orientation of the whole ligand. For the alignments in D₂, it was observed that ligands make a “bend” toward the TM2/7 cleft at the heterocyclic appendage end. For ligands with a shorter spacer, the bent orientation seems to result in a tighter fit to the binding pocket. Those with a longer alkyl spacer make a sharper turn, possibly disfavoring the adoption of this orientation. Multiple SAR studies have found that shortening of the spacer resulted in preferential D₂ binding over D₃.^{3,7,8,12–14} The alignments produced from our models again suggest that the smaller ligands are more D₂ selective because of the shallower binding pocket of D₂. In the models for D₃, the binding site in the TM5/6 region

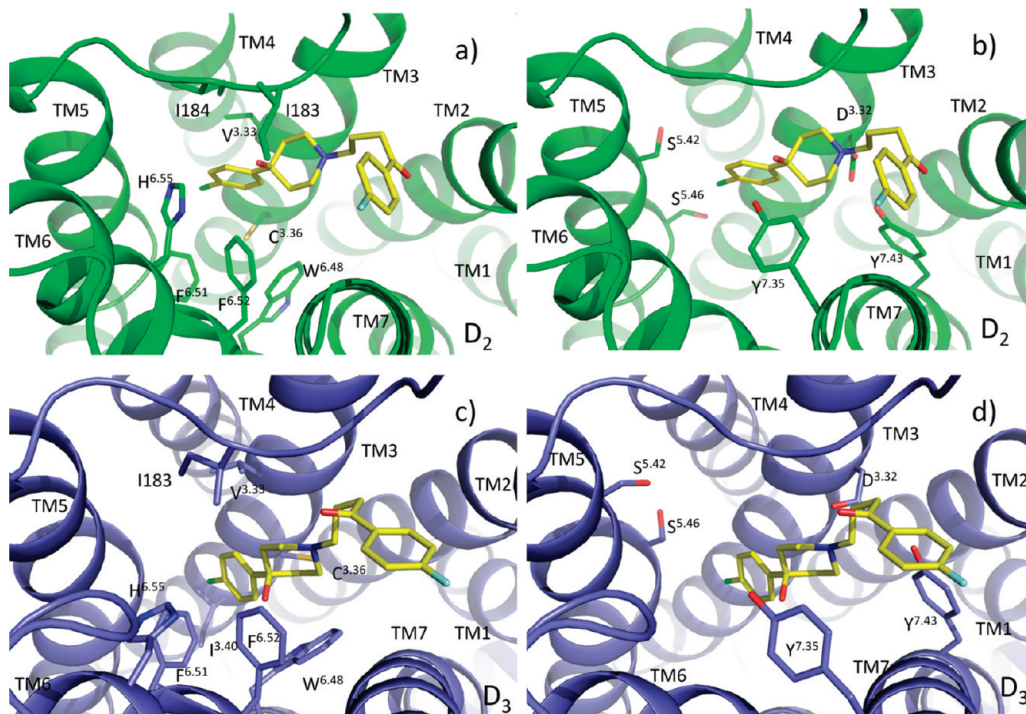


Figure 5. Interactions of the receptor residues with haloperidol. The important residues are shown as stick models and labeled. (a) Hydrophobic interactions on D₂; (b) hydrogen bonding on D₂; (c) hydrophobic interactions on D₃; (d) hydrogen bonding on D₃.

is deeper. Therefore, the ligands penetrate more and adopt a more extended, linear conformation, making extensive interactions with the receptor residues. This may be the basis for why longer ligands tend to be more selective for D₃ compared to D₂ receptors.

3D-QSAR Models. The CoMFA and CoMSIA models were derived from the 121 ligands in the training set, for D₂ and D₃ receptors, respectively. To explore the effect of various fields on the predictability of the models, three separate CoMSIA models were built using different combinations of steric, electrostatic, hydrophobic, and hydrogen bond (donor and acceptor) fields. The PLS analysis results are summarized in Table 3. For the D₂ models, the statistical indices are reasonably high, with CoMSIA model 3 having the best cross-validated q^2 . This indicates that all models have good predictability. For the D₃ models, the three COMSIA models have even higher cross-validated q^2 values, demonstrating their predictive power. The high statistical values indicate that the alignment reflects the natural binding conformations of the ligands, and it lays the foundation of a reliable QSAR model.

Validation is always a crucial step in QSAR modeling. It has been found that the widely accepted LOO cross-validated q^2 is inadequate to assess the predictive ability of the QSAR models,⁴¹ since some models based on the training set with randomized affinities appeared to have high q^2 values but showed low predictive power to an external test set. This could be explained by a chance correlation or structural redundancy.⁵² Therefore, we set out to validate the models by predicting the binding affinities of the compounds in the test set using the above models. The results are reported in Table 4. A set of rigorous criteria has been suggested for the evaluation of a QSAR model, including calculating the coefficients of determination⁴⁴ (R_0^2 and $R_0'^2$) and slopes of regression (K and K') when forcing the intercept to pass through the origin. A QSAR model has been concluded to

have an acceptable predictive power if the following conditions are satisfied.^{41–43} (i) $q^2 > 0.5$; (ii) $r_{\text{test}}^2 > 0.6$; (iii) $(r_{\text{test}}^2 - R_0^2)/r_{\text{test}}^2 < 0.1$ and $0.85 \leq K \leq 1.15$ or $(r_{\text{test}}^2 - R_0'^2)/r_{\text{test}}^2 < 0.1$ and $0.85 \leq K' \leq 1.15$; (iv) $|R_0^2 - R_0'^2| < 0.3$. Therefore, the predicted values of the test set in Table 4 were also used to calculate R_0^2 , $R_0'^2$, K , and K' as reported in Table 5. Figure 7 shows the corresponding plots of the calculated versus the experimental values for the training set and the test set of the three models for D₂ and D₃, respectively. For the test set, the fittings between the predictive versus experimental values and experimental versus predictive values (the calculation of R_0^2 , $R_0'^2$, K , and K') are illustrated in Figures 8 and 9 for the D₂ and D₃ models, respectively. It is clear that all of the above conditions are satisfied by each model in our studies, for both D₂ and D₃ receptor subtypes. Since they behave almost equally well for the external test set in predicting the ligands' binding affinity, any of the models could be applied alternatively in evaluating a new compound's activity for a thorough prediction. If all of the models collectively suggest that a compound has high affinity for a particular receptor subtype, it is very likely to be a potent ligand.

To further validate the models, different selections of molecules making up the test and training sets or different test set and training set sizes were also evaluated. Very similar QSAR models, with about the same predictive power, were produced (results not shown), indicating that the models are robust and the results are informative for interpreting molecular interactions.

Figures 10 and 11 show illustrations of the molecular fields from the model which contains all of the contributing factors (CoMSIA 1) for D₂ and D₃ receptors, respectively, with the ligand haloperidol rendered within the fields. From the D₂ receptor models, the contribution breakdown suggests that hydrophobic interactions are the major determinant factor for the compounds' binding affinities, while steric interac-

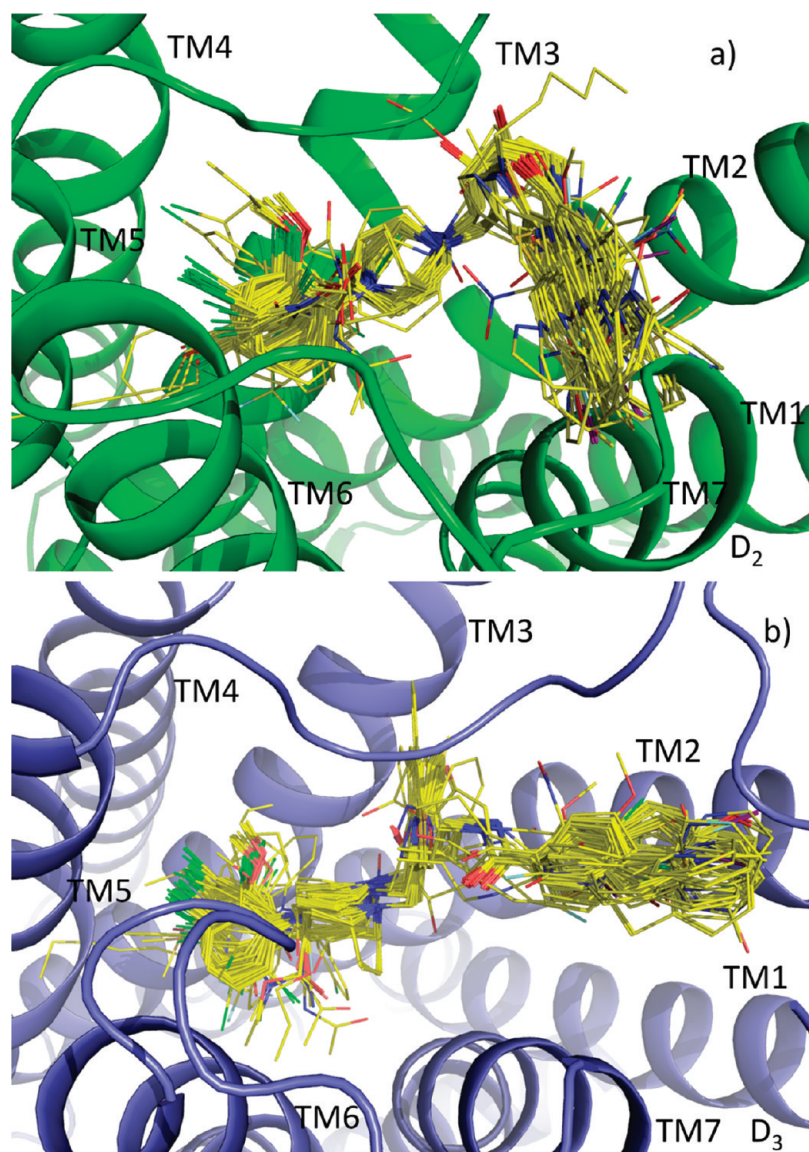


Figure 6. Alignments for the 163 ligands obtained by ROCS shown in the binding site on the receptors. Atom color scheme: C, yellow; O, red; N, blue; S, orange; Cl, yellow; F, gray; Br, maroon; and I, purple. Hydrogen atoms are not displayed.

Table 3. Results from CoMSIA Models for the Training Set of the Two Alignments on D₂/D₃ Receptors^a

receptor	model	<i>r</i> ²	<i>q</i> ²	SEE	F	PC	% contribution			
							steric	electrostatic	hydrophobic	H bond (D/A)
D ₂	CoMSIA1	0.896	0.509	0.267	139.7	7	9.0	14.7	33.7	17.8/24.7
	CoMSIA2	0.878	0.552	0.288	117.7	7	11.2	20.5	41.8	26.5/-
	CoMSIA3	0.839	0.586	0.330	100.0	6	14.1	31.1	54.8	
D ₃	CoMSIA1	0.926	0.752	0.349	289.3	5	9.0	15.4	26.2	28.4/21.0
	CoMSIA2	0.876	0.757	0.449	206.5	4	19.0	32.4	48.5	
	CoMSIA3	0.844	0.759	0.502	212.1	3	42.6	57.4		

^a *r*²: non-cross-validated correlation coefficient. *q*²: cross-validated correlation coefficient. SEE: standard error of estimation. PC: principal component number. D: hydrogen bond donor. A: hydrogen bond acceptor.

tions play a minimal role. For the D₃ models, although less important, hydrophobic interactions are still the most important contribution to the compounds' binding. Hydrogen bonding also contributes a large portion to the binding affinity in both D₂ and D₃, which may reinforce the binding selectivity of some ligands. A side by side comparison of the steric maps shows that the binding crevice is deeper in D₃, as it favors more bulky groups all around and deep beneath the *para*-chlorophenyl ring. In contrast, the D₂ site

only favors some substitutions on the ring, or along the spacer on the heterocyclic appendage (*para*-fluorophenyl ring), since the site is more open in this region. The hydrophobic maps show that the ligands are intrinsically hydrophobic, with a little preference for hydrophilic properties inside the cavity. It is not desirable for the D₂ receptor to have more hydrogen bond donating substituents near the hydroxyl substituent on the piperidinium group of haloperidol, since the hydroxyl group could be a donor interacting with the D₂

Table 4. Predicted Affinities of the Test Set Utilizing the Three CoMSIA Models

ligand	D ₂						D ₃								
	CoMSIA1			CoMSIA2		CoMSIA3		CoMSIA1			CoMSIA2		CoMSIA3		
	exp. ^a pK _i	pred. ^b	resi. ^c	pred.	resi.	pred.	resi.	ligand	exp. pK _i	pred.	resi.	pred.	resi.	pred.	resi.
6	8.638	7.962	-0.676	8.010	-0.628	8.211	-0.428	2	6.983	6.389	-0.595	6.380	-0.603	6.187	-0.796
14	6.693	6.432	-0.260	6.319	-0.373	6.433	-0.260	3	6.602	6.479	-0.123	6.491	-0.111	6.351	-0.251
17	7.499	7.682	0.183	7.831	0.332	7.489	-0.010	4	6.690	6.449	-0.241	6.374	-0.316	6.155	-0.536
22	7.668	7.729	0.061	7.676	0.009	7.730	0.063	8	6.195	5.913	-0.282	6.161	-0.034	6.013	-0.182
23	7.264	7.540	0.276	7.610	0.347	7.392	0.129	20	8.377	8.843	0.466	8.984	0.607	9.001	0.625
29	7.943	7.592	-0.351	7.631	-0.313	7.699	-0.244	21	9.046	8.947	-0.099	9.224	0.178	9.213	0.167
31	7.403	7.329	-0.075	7.322	-0.082	7.413	0.010	25	8.886	8.686	-0.200	8.944	0.058	8.894	0.008
40	6.364	6.494	0.131	6.351	-0.012	6.415	0.052	33	9.155	9.180	0.025	9.147	-0.008	8.952	-0.203
43	7.327	6.486	-0.841	6.464	-0.863	6.404	-0.923	39	8.583	8.581	-0.002	8.787	0.203	8.783	0.199
46	5.975	6.333	0.358	6.249	0.274	6.278	0.303	55	9.585	9.094	-0.491	8.973	-0.612	8.820	-0.765
50	6.206	6.409	0.203	6.422	0.216	6.604	0.397	58	8.197	7.233	-0.965	7.344	-0.854	7.364	-0.834
59	6.264	6.242	-0.022	5.998	-0.266	6.190	-0.074	64	7.072	7.274	0.202	7.505	0.433	7.369	0.297
62	5.684	6.616	0.932	6.697	1.013	6.632	0.948	68	7.747	8.700	0.953	8.222	0.475	7.869	0.122
67	7.889	7.886	-0.003	7.905	0.016	7.810	-0.080	69	6.366	7.928	1.562	7.707	1.341	7.580	1.214
68	7.526	7.752	0.226	7.900	0.374	7.795	0.269	72	7.492	8.143	0.651	8.155	0.663	8.442	0.950
70	8.975	8.677	-0.298	8.685	-0.290	8.624	-0.351	75	8.678	8.367	-0.311	8.496	-0.182	8.727	0.050
73	8.310	8.326	0.017	8.273	-0.037	8.175	-0.135	76	9.432	8.939	-0.493	8.763	-0.669	8.989	-0.443
76	8.921	8.204	-0.717	8.142	-0.779	8.252	-0.669	77	8.076	8.427	0.352	8.430	0.354	8.453	0.377
82	7.030	7.164	0.134	7.081	0.051	6.957	-0.073	80	9.398	9.614	0.216	9.522	0.124	9.342	-0.056
85	7.627	7.139	-0.488	7.010	-0.617	7.040	-0.587	81	8.824	8.791	-0.033	8.638	-0.186	8.929	0.105
86	6.979	7.004	0.026	6.892	-0.087	6.777	-0.202	89	7.308	7.360	0.052	7.030	-0.278	6.944	-0.364
88	7.588	7.190	-0.399	7.109	-0.480	6.999	-0.589	91	8.921	8.501	-0.419	8.743	-0.178	8.948	0.027
90	7.161	7.333	0.172	7.303	0.141	7.042	-0.119	92	8.523	8.973	0.451	8.598	0.075	8.705	0.182
93	6.496	6.150	-0.346	6.226	-0.270	6.256	-0.240	93	8.745	8.722	-0.023	8.455	-0.290	8.698	-0.047
95	6.604	6.333	-0.270	6.491	-0.113	6.738	0.134	96	7.932	7.664	-0.268	8.429	0.497	8.327	0.395
97	7.547	7.667	0.120	7.302	-0.245	7.225	-0.322	97	9.301	9.326	0.025	9.250	-0.051	8.963	-0.338
103	7.583	6.738	-0.845	6.616	-0.967	6.338	-1.245	99	8.886	8.501	-0.385	8.770	-0.116	8.866	-0.020
107	6.896	6.992	0.096	6.875	-0.021	6.786	-0.110	100	9.000	8.416	-0.584	9.126	0.126	8.876	-0.124
109	6.752	6.674	-0.078	6.591	-0.161	6.442	-0.310	101	6.796	8.539	1.743	8.988	2.192	8.822	2.026
114	5.370	5.139	-0.232	4.883	-0.487	4.996	-0.374	109	5.672	6.017	0.345	6.028	0.357	6.018	0.347
117	7.080	6.579	-0.501	6.748	-0.333	7.029	-0.051	113	5.261	6.126	0.865	5.933	0.672	6.315	1.054
120	7.222	7.214	-0.008	6.848	-0.374	6.840	-0.382	119	6.165	6.915	0.750	6.667	0.502	6.438	0.273
126	7.813	7.462	-0.350	7.526	-0.287	7.533	-0.280	123	6.975	6.113	-0.862	6.205	-0.770	6.157	-0.818
131	7.268	7.627	0.359	7.807	0.540	7.769	0.501	131	6.857	7.441	0.584	7.359	0.502	7.322	0.465
137	7.991	8.065	0.073	8.007	0.016	8.025	0.033	133	6.312	7.611	1.300	7.028	0.717	6.778	0.466
141	7.551	8.319	0.767	8.258	0.706	8.225	0.674	143	9.222	8.258	-0.964	8.604	-0.617	8.594	-0.628
142	7.451	7.429	-0.022	7.412	-0.039	7.357	-0.094	148	8.469	8.616	0.147	8.814	0.345	8.611	0.142
146	8.181	7.672	-0.509	7.864	-0.317	7.934	-0.247	149	8.638	8.635	-0.003	8.651	0.012	8.536	-0.102
154	7.708	7.298	-0.409	7.363	-0.345	7.530	-0.178	154	8.602	8.687	0.084	8.649	0.047	8.546	-0.056
159	8.097	7.942	-0.155	7.618	-0.478	7.624	-0.473	159	9.523	9.231	-0.292	8.940	-0.583	8.875	-0.648
161	6.827	7.417	0.591	7.287	0.460	7.441	0.615	163	9.097	8.713	-0.384	8.590	-0.507	8.540	-0.557

^a exp. refers to experimentally measured pK_i. ^b pred. refers to predicted pK_i. ^c resi. refers to the corresponding difference between the predicted and measured pK_i.

Table 5. Statistical Results from the Three CoMSIA Models Each for the Two Receptors

receptor	model	r^2	q^2	r_{test}^2	R_0^2	K	$(r_{test}^2 - R_0^2)/r_{test}^2$	$R_0'^2$	K'	$(r_{test}^2 - R_0'^2)/r_{test}^2$	$ R_0^2 - R_0'^2 $
		CoMSIA1	0.896	0.509	0.757	0.710	0.987	0.062	0.754	1.010	0.004
D ₂	CoMSIA2	0.878	0.552	0.740	0.710	0.982	0.041	0.729	1.015	0.015	0.019
	CoMSIA3	0.839	0.586	0.740	0.699	0.981	0.055	0.734	1.016	0.008	0.035
	CoMSIA1	0.926	0.752	0.733	0.639	1.003	0.128	0.733	0.992	0.000	0.094
	CoMSIA2	0.876	0.757	0.765	0.698	1.006	0.088	0.765	0.989	0.000	0.067
D ₃	CoMSIA3	0.844	0.759	0.764	0.710	1.001	0.071	0.764	0.994	0.001	0.054

receptor (Y^{7,35}) with high affinity. On D₃, this interaction is absent, consistent with previous receptor models, showing that a hydroxyl substituent on the piperidium ring is a critical pharmacophore for the selectivity between the two receptor subtypes. The CoMSIA results agree with the receptor models in probing the difference of the binding sites and mapping the molecular fingerprints of the ligands that discriminate between the two receptors. Furthermore, it provides valuable information

to optimize the lead compounds in order to develop more potent and/or selective ligands.

Previously, only limited molecular modeling studies have been reported on the selectivity of dopamine receptor ligands. These studies have focused on the D₂ receptor, using either structure or ligand-based methods. In the earlier reported work, the 3D models of the D₂ receptors were constructed either by using the bovine rhodopsin structure as the template

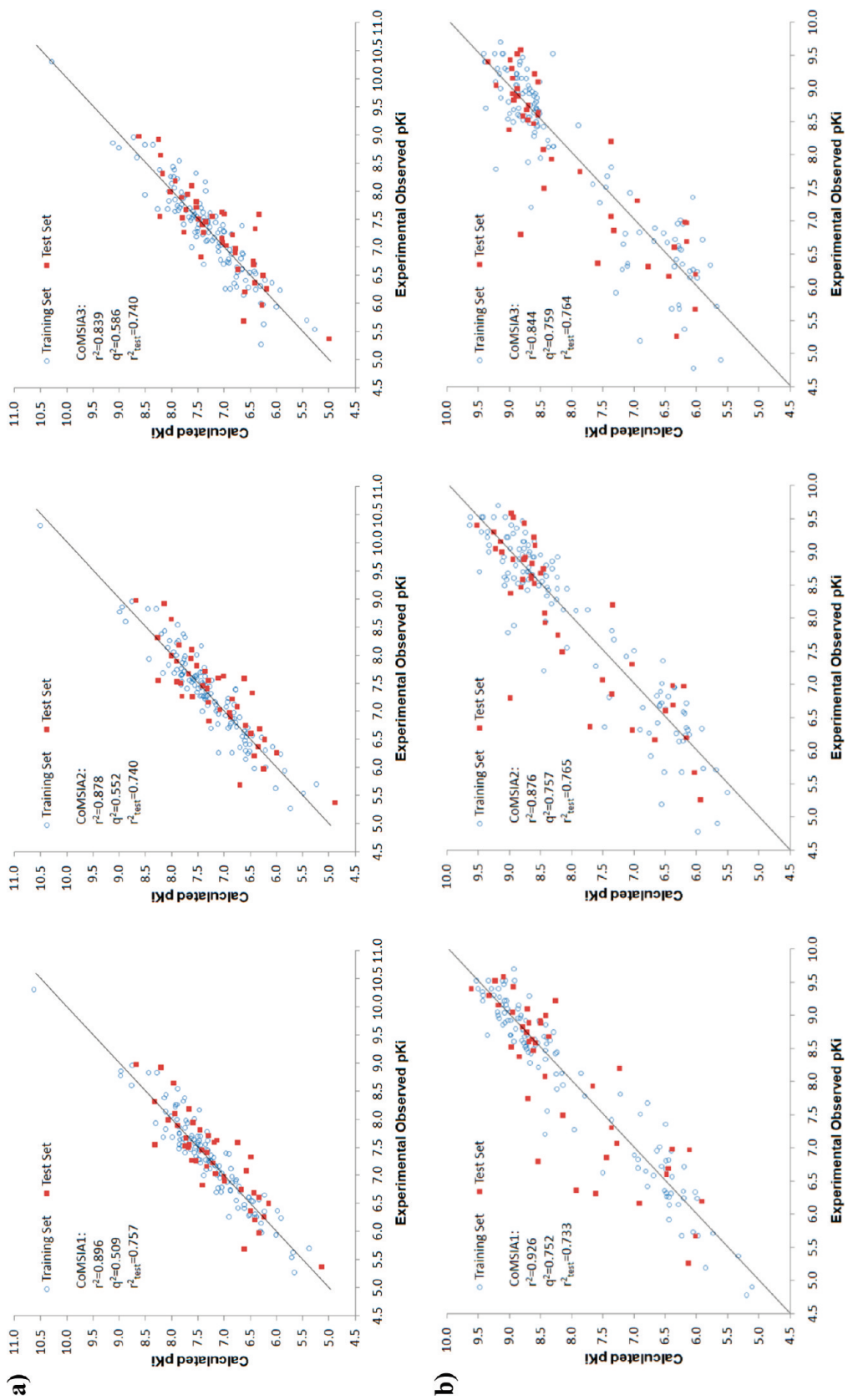


Figure 7. QSAR modeling. Experimentally measured pK_i versus the fitted values for the training-set compounds (\circ) and the predicted values for the test-set compounds (\square) from CoMSIA models 1, 2, and 3 for (a) D_2 and (b) D_3 . All plots begin at the origin; the axes have been truncated for improved graphical presentation.

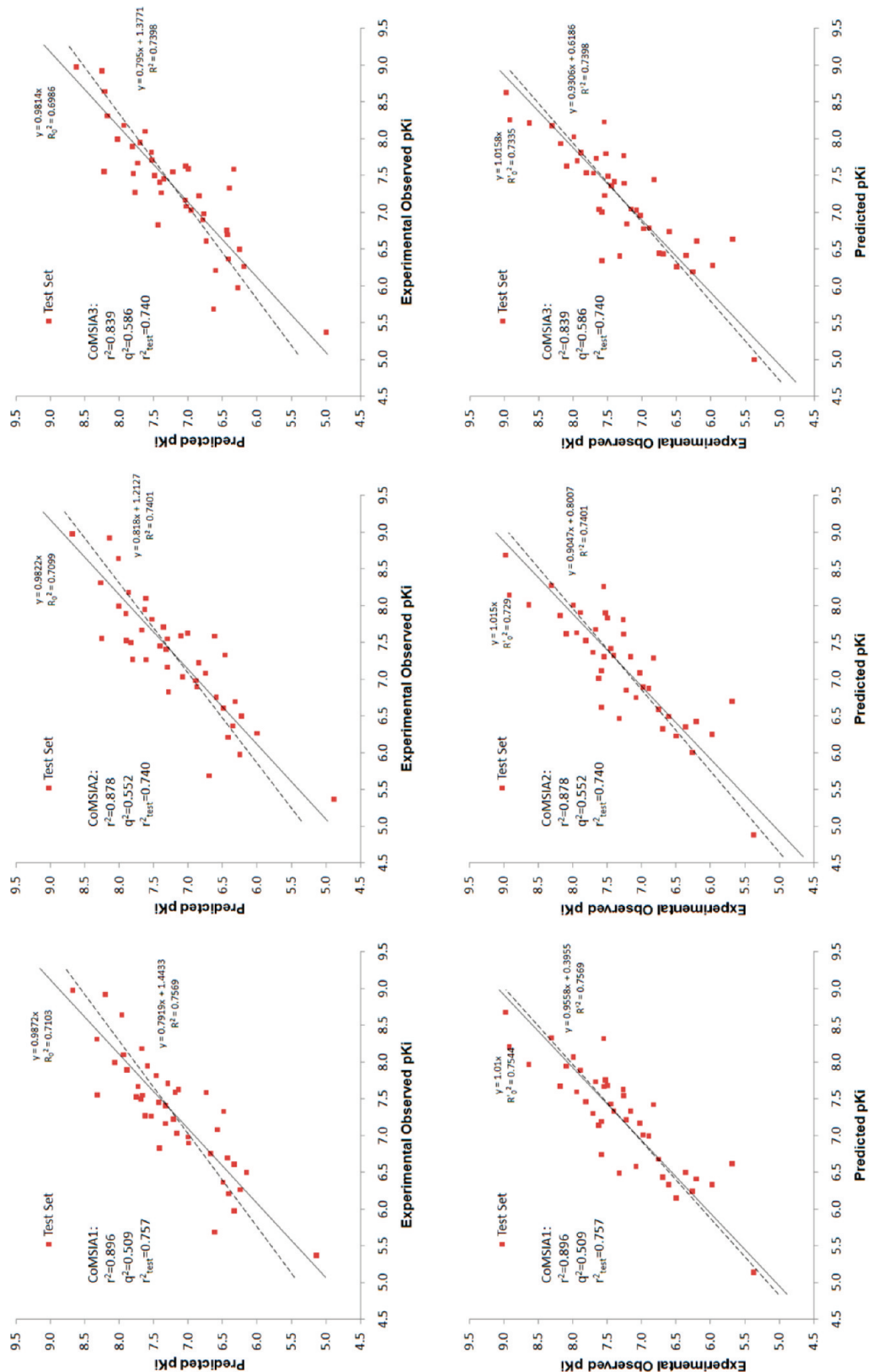


Figure 8. QSAR modeling. Observed vs predicted and predicted vs observed pK_i by CoMSIA models 1, 2, and 3, using the test set. Two regression results, with (solid line) or without (dashed line) forcing the intercept to be zero, are shown for each data set for D_2 . All plots begin at the origin; the axes have been truncated for improved graphical presentation.

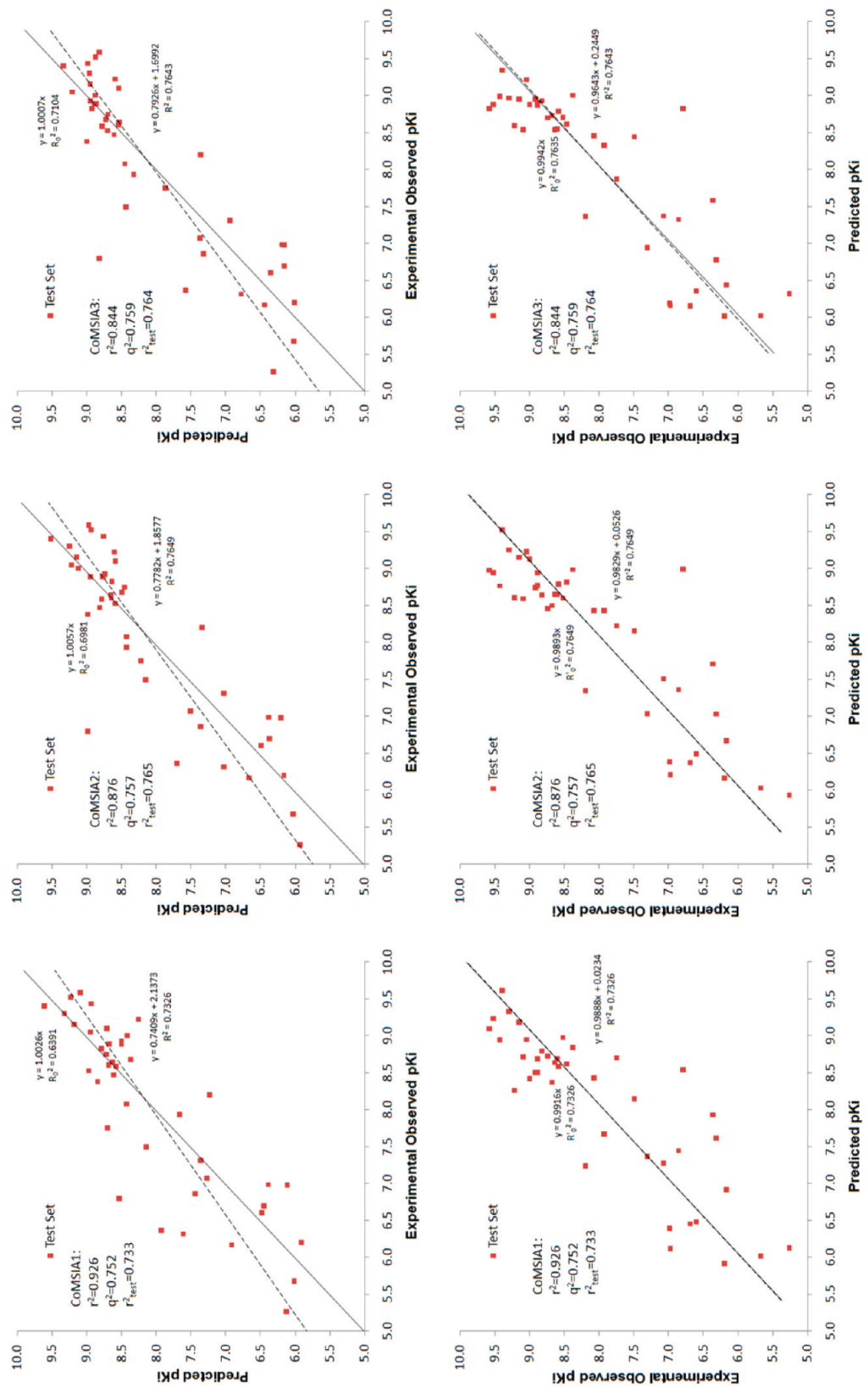


Figure 9. QSAR modeling. Observed vs predicted and predicted vs observed pK_i by CoMSIA models 1, 2, and 3, using the test set. Two regression results, with (solid line) or without (dashed line) forcing the intercept to be zero, are shown for each data set for D_3 . All plots begin at the origin; the axes have been truncated for improved graphical presentation.

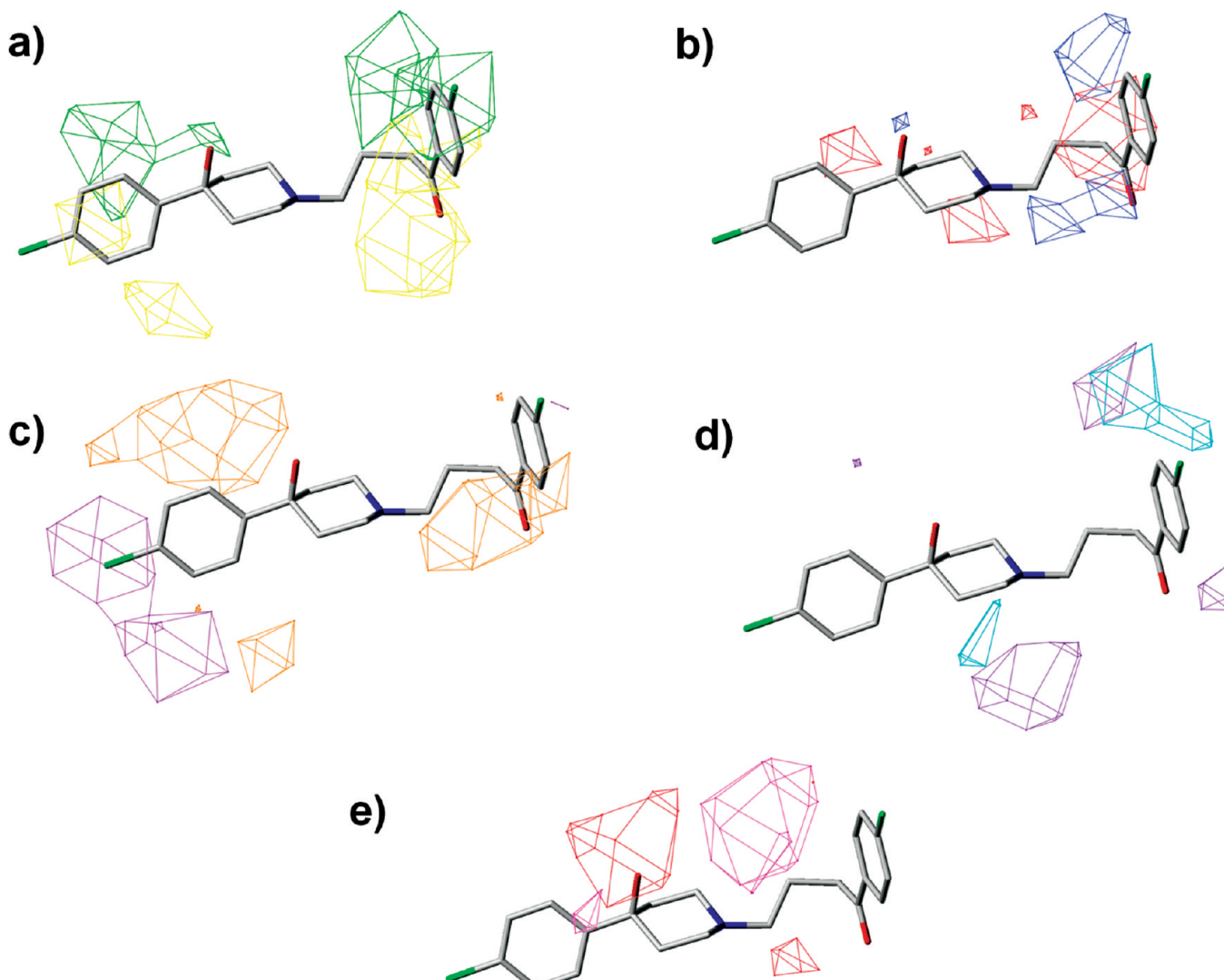


Figure 10. Molecular field maps derived from the model (CoMSIA1) of D₂, with ligand haloperidol illustrated. Contours of the steric map are shown in a; the electrostatic map in b; hydrophobic map in c; hydrogen bond donor in d; and hydrogen bond acceptor in e. Atom color scheme: C, gray (3) or green (34); O, red; N, blue; S, yellow. Hydrogen atoms are not displayed. The contours are displayed at the 80% favored and 20% disfavored level. Increased binding affinity is correlated with more bulk near green, less bulk near yellow in the steric map; more positive charge near blue, more negative charge near red in the electrostatic map; more hydrophobic near orange, less hydrophobic near violet in the hydrophobic map; more hydrogen bond donor (on the receptor) near cyan, less hydrogen bond donor near purple in the hydrogen bond donor map; more hydrogen bond acceptor (on the receptor) near magenta, and less hydrogen bond acceptor near red in the hydrogen bond acceptor map.

for homology modeling^{47,51,53,54} or using *ab initio* theoretical and computational techniques.⁵⁵ The resultant models were, therefore, not accurate enough for evaluating receptor–ligand interactions quantitatively. Even for the homology models based on the more closely related β₂-adrenergic receptor,^{13,23,24,56} comparing the D₂ receptor structure with the highly homologous D₃ receptor would be problematic without extensive model refinements, since the difference between the two receptor subtypes could be subtle. The analysis of our refined D₂/D₃ models suggests that substantial structural changes are observed in the refinement process, indicating that comprehensive refinements are necessary to discern the difference at the binding sites. In the ligand-based studies, most of the QSAR models were built from training sets consisting of a small number of ligands or structurally very similar ligands, not thoroughly validated, or not very statistically predictive.^{14,57–59}

CONCLUSIONS

In this work, we have utilized both structure- and ligand-based approaches of homology modeling and 3D-QSAR to explore the intermolecular interactions of a large library of ligands with dopamine D₂/D₃ receptors. Our goal was to establish molecular models capable of explaining the mechanism of binding selectivity for the two highly homologous receptor subtypes. The combination of the two approaches and utilization of a large diverse compound library allowed the exploration of the molecular basis of subtype selectivity, by (1) obtaining reliable 3D models of prototypical ligand bound D₂/D₃ receptor complexes, (2) using the ligand bound conformation to guide the alignments for the compound library, and (3) deriving highly predictive QSAR models based on the ligand alignments.

The developed QSAR models included ligands with diverse structures, and highly variable binding affinities spanning 5

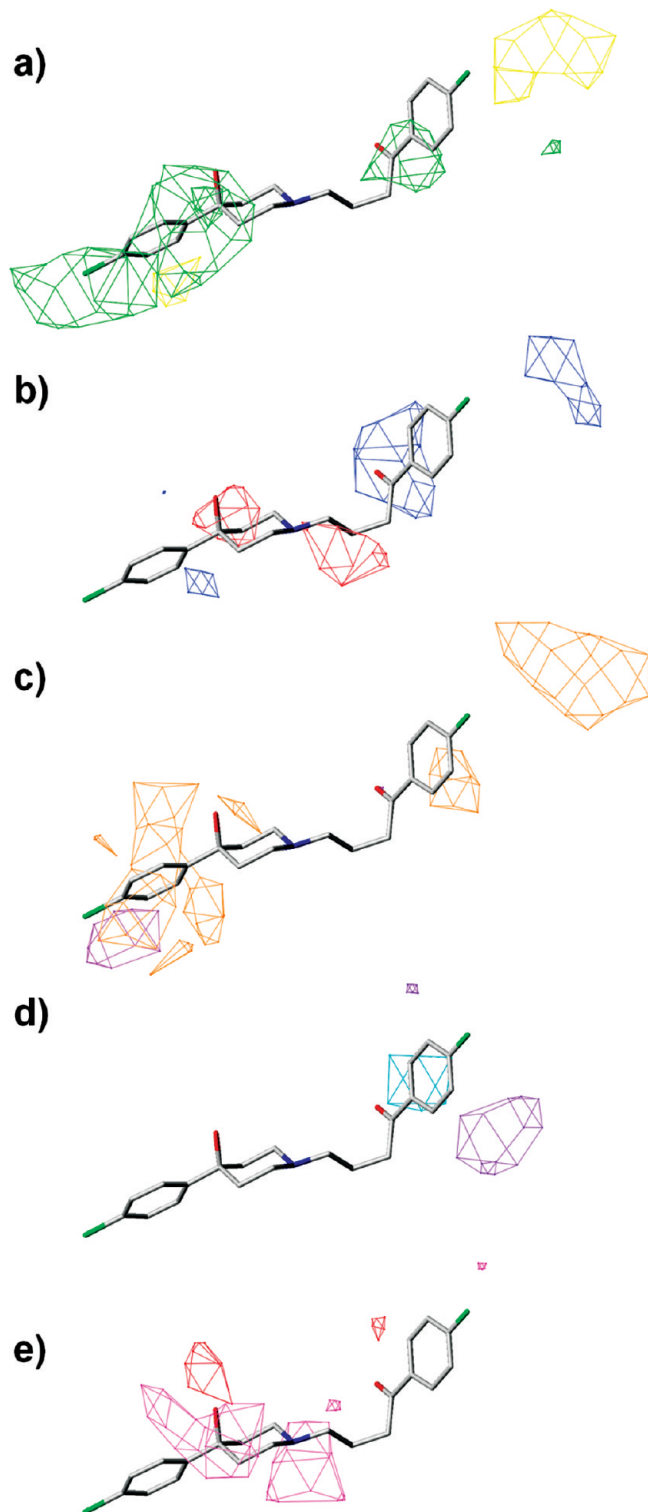


Figure 11. Molecular field maps derived from the model (CoMSIA1) of D_3 , with ligand haloperidol illustrated. Details are the same as in Figure 10.

orders of magnitude (mM to sub-nM range), while still achieving excellent results correlating the 3D molecular fields with their binding affinities on the two receptors. Our work sheds light on how different sequence compositions, especially in the extracellular loop regions of the receptors, can lead to differences in size and contouring properties of the orthosteric sites, which in turn results in recognition preferences. The work should be beneficial in seeking more potent and/or selective dopamine D_2/D_3 receptor ligands, by rationally optimizing the

functional groups on the current lead compounds to achieve better binding, or using the receptor models for virtual screening of large compound databases for new scaffolds. It is also expandable to other dopamine receptor subtypes in the pursuit of small molecular modulators and/or imaging agents for neurologic disorders.

ACKNOWLEDGMENT

This work was support by the following grants: R01 DA13584-03S1 (R.R.L.), R01 MH81281 (R.H.M.), R01 DA23957-01 (R.R.L. and R.H.M.), DA029840-01 (R.H.M. and R.R.L.), DA16181 (R.H.M. and R.R.L.).

Supporting Information Available: The structures of the receptor models and the molecules in their alignments used in the QSAR study are available as PDB and (zipped) mol2 files, respectively. A supporting Table 1 containing the complete set of ligand structures and K_i values is also available. This material is available free of charge via the Internet at <http://pubs.acs.org>.

REFERENCES AND NOTES

- Girault, J. A.; Greengard, P. The neurobiology of dopamine signaling. *Arch. Neurol.* **2004**, *61*, 641.
- Zhang, A.; Neumeyer, J. L.; Baldessarini, R. J. Recent progress in development of dopamine receptor subtype-selective agents: potential therapeutics for neurological and psychiatric disorders. *Chem. Rev.* **2007**, *107*, 274.
- Boeckler, F.; Gmeiner, P. Dopamine D_3 receptor ligands: recent advances in the control of subtype selectivity and intrinsic activity. *Biochim. Biophys. Acta* **2007**, *1768*, 871.
- Chu, W.; Tu, Z.; McElveen, E.; Xu, J.; Taylor, M.; Luedtke, R. R.; Mach, R. H. Synthesis and in vitro binding of N-phenyl piperazine analogs as potential dopamine D_3 receptor ligands. *Bioorg. Med. Chem.* **2005**, *13*, 77.
- Grundt, P.; Carlson, E. E.; Cao, J.; Bennett, C. J.; McElveen, E.; Taylor, M.; Luedtke, R. R.; Newman, A. H. Novel heterocyclic trans olefin analogues of N-[4-(4-(2,3-dichlorophenyl)piperazin-1-yl)butyl]arylcaboxamides as selective probes with high affinity for the dopamine D_3 receptor. *J. Med. Chem.* **2005**, *48*, 839.
- Vangveravong, S.; McElveen, E.; Taylor, M.; Xu, J.; Tu, Z.; Luedtke, R. R.; Mach, R. H. Synthesis and characterization of selective dopamine D_2 receptor antagonists. *Bioorg. Med. Chem.* **2006**, *14*, 815.
- Grundt, P.; Husband, S. L.; Luedtke, R. R.; Taylor, M.; Newman, A. H. Analogues of the dopamine D_2 receptor antagonist L741,626: Binding, function, and SAR. *Bioorg. Med. Chem. Lett.* **2007**, *17*, 745.
- Paul, N. M.; Taylor, M.; Kumar, R.; Deschamps, J. R.; Luedtke, R. R.; Newman, A. H. Structure-activity relationships for novel series of dopamine D_2 -like receptor ligands based on N-substituted 3-aryl-8-azabicyclo[3.2.1]octan-3-ol. *J. Med. Chem.* **2008**, *51*, 6095.
- Newman, A. H.; Grundt, P.; Cyriac, G.; Deschamps, J. R.; Taylor, M.; Kumar, R.; Ho, D.; Luedtke, R. R. N-(4-(4-(2,3-dichloro- or 2-methoxyphenyl)piperazin-1-yl)butyl)heterobiarylcarboxamides with functionalized linking chains as high affinity and enantioselective D_3 receptor antagonists. *J. Med. Chem.* **2009**, *52*, 2559.
- Bettinetti, L.; Schlotter, K.; Hubner, H.; Gmeiner, P. Interactive SAR studies: rational discovery of super-potent and highly selective dopamine D_3 receptor antagonists and partial agonists. *J. Med. Chem.* **2002**, *45*, 4594.
- Hocke, C.; Prante, O.; Lober, S.; Hubner, H.; Gmeiner, P.; Kuwert, T. Synthesis and radioiodination of selective ligands for the dopamine D_3 receptor subtype. *Bioorg. Med. Chem. Lett.* **2004**, *14*, 3963.
- Bettinetti, L.; Hubner, H.; Gmeiner, P. Chirospecific and subtype selective dopamine receptor binding of heterocyclic methoxynaphthamide analogs. *Arch. Pharm. (Weinheim)* **2005**, *338*, 276.
- Ehrlich, K.; Gotz, A.; Bollinger, S.; Tschammer, N.; Bettinetti, L.; Harterich, S.; Hubner, H.; Lanig, H.; Gmeiner, P. Dopamine D_2 , D_3 , and D_4 selective phenylpiperazines as molecular probes to explore the origins of subtype specific receptor binding. *J. Med. Chem.* **2009**, *52*, 4923.
- Salama, I.; Hocke, C.; Utz, W.; Prante, O.; Boeckler, F.; Hubner, H.; Kuwert, T.; Gmeiner, P. Structure-selectivity investigations of D_2 -like receptor ligands by CoMFA and CoMSIA guiding the discovery of D_3 selective PET radioligands. *J. Med. Chem.* **2007**, *50*, 489.

- (15) Cherezov, V.; Rosenbaum, D. M.; Hanson, M. A.; Rasmussen, S. G.; Thian, F. S.; Kobilka, T. S.; Choi, H. J.; Kuhn, P.; Weis, W. I.; Kobilka, B. K.; Stevens, R. C. High-resolution crystal structure of an engineered human beta2-adrenergic G protein-coupled receptor. *Science* **2007**, *318*, 1258.
- (16) Rasmussen, S. G.; Choi, H. J.; Rosenbaum, D. M.; Kobilka, T. S.; Thian, F. S.; Edwards, P. C.; Burghammer, M.; Ratnala, V. R.; Sanishvili, R.; Fischetti, R. F.; Schertler, G. F.; Weis, W. I.; Kobilka, B. K. Crystal structure of the human beta2 adrenergic G-protein-coupled receptor. *Nature* **2007**, *450*, 383.
- (17) Rosenbaum, D. M.; Cherezov, V.; Hanson, M. A.; Rasmussen, S. G.; Thian, F. S.; Kobilka, T. S.; Choi, H. J.; Yao, X. J.; Weis, W. I.; Stevens, R. C.; Kobilka, B. K. GPCR engineering yields high-resolution structural insights into beta2-adrenergic receptor function. *Science* **2007**, *318*, 1266.
- (18) Palczewski, K.; Kumada, T.; Hori, T.; Behnke, C. A.; Motoshima, H.; Fox, B. A.; Le Trong, I.; Teller, D. C.; Okada, T.; Stenkamp, R. E.; Yamamoto, M.; Miyano, M. Crystal structure of rhodopsin: A G protein-coupled receptor. *Science* **2000**, *289*, 739.
- (19) Okada, T.; Fujiyoshi, Y.; Silow, M.; Navarro, J.; Landau, E. M.; Shichida, Y. Functional role of internal water molecules in rhodopsin revealed by X-ray crystallography. *Proc. Natl. Acad. Sci. U. S. A.* **2002**, *99*, 5982.
- (20) Okada, T.; Sugihara, M.; Bondar, A. N.; Elstner, M.; Entel, P.; Buss, V. The retinal conformation and its environment in rhodopsin in light of a new 2.2 Å crystal structure. *J. Mol. Biol.* **2004**, *342*, 571.
- (21) Michino, M.; Abola, E.; Brooks, C. L., III; Dixon, J. S.; Moult, J.; Stevens, R. C. Community-wide assessment of GPCR structure modelling and ligand docking: GPCR Dock 2008. *Nat. Rev. Drug Discovery* **2009**, *8*, 455.
- (22) Topiol, S.; Sabio, M. X-ray structure breakthroughs in the GPCR transmembrane region. *Biochem. Pharmacol.* **2009**, *78*, 11.
- (23) Selent, J.; Lopez, L.; Sanz, F.; Pastor, M. Multi-receptor binding profile of clozapine and olanzapine: a structural study based on the new beta2 adrenergic receptor template. *ChemMedChem* **2008**, *3*, 1194.
- (24) McRobb, F. M.; Capuano, B.; Crosby, I. T.; Chalmers, D. K.; Yuriev, E. Homology modeling and docking evaluation of aminergic G protein-coupled receptors. *J. Chem. Inf. Model.* **2010**, *50*, 626.
- (25) Marti-Renom, M. A.; Stuart, A. C.; Fiser, A.; Sanchez, R.; Melo, F.; Sali, A. Comparative protein structure modeling of genes and genomes. *Annu. Rev. Biophys. Biomol. Struct.* **2000**, *29*, 291.
- (26) Larkin, M. A.; Blackshields, G.; Brown, N. P.; Chenna, R.; McGgettigan, P. A.; McWilliam, H.; Valentin, F.; Wallace, I. M.; Wilm, A.; Lopez, R.; Thompson, J. D.; Gibson, T. J.; Higgins, D. G. Clustal W and Clustal X version 2.0. *Bioinformatics* **2007**, *23*, 2947.
- (27) Shi, L.; Javitch, J. A. The binding site of aminergic G protein-coupled receptors: the transmembrane segments and second extracellular loop. *Annu. Rev. Pharmacol. Toxicol.* **2002**, *42*, 437.
- (28) SYBYL, 8.1; Tripos International: St. Louis, MO, 2009.
- (29) Caves, L. S.; Evanseck, J. D.; Karplus, M. Locally accessible conformations of proteins: multiple molecular dynamics simulations of crambin. *Protein Sci.* **1998**, *7*, 649.
- (30) Humphrey, W.; Dalke, A.; Schulten, K. VMD: visual molecular dynamics. *J. Mol. Graph.* **1996**, *14*, 33.
- (31) Phillips, J. C.; Braun, R.; Wang, W.; Gumbart, J.; Tajkhorshid, E.; Villa, E.; Chipot, C.; Skeel, R. D.; Kale, L.; Schulten, K. Scalable molecular dynamics with NAMD. *J. Comput. Chem.* **2005**, *26*, 1781.
- (32) MacKerell, A. D.; Bashford, D.; Bellott, M.; Dunbrack, R. L.; Evanseck, J. D.; Field, M. J.; Fischer, S.; Gao, J.; Guo, H.; Ha, S.; Joseph-McCarthy, D.; Kuchnir, L.; Kuczera, K.; Lau, F. T. K.; Mattos, C.; Michnick, S.; Ngo, T.; Nguyen, D. T.; Prodhom, B.; Reiher, W. E.; Roux, B.; Schlenkrich, M.; Smith, J. C.; Stote, R.; Straub, J.; Watanabe, M.; Wiorkiewicz-Kuczera, J.; Yin, D.; Karplus, M. All-atom empirical potential for molecular modeling and dynamics studies of proteins. *J. Phys. Chem. B* **1998**, *102*, 3586.
- (33) MacKerell, A. D., Jr.; Feig, M.; Brooks, C. L., III. Extending the treatment of backbone energetics in protein force fields: limitations of gas-phase quantum mechanics in reproducing protein conformational distributions in molecular dynamics simulations. *J. Comput. Chem.* **2004**, *25*, 1400.
- (34) Wang, H. L.; Cheng, X.; Taylor, P.; McCammon, J. A.; Sine, S. M. Control of cation permeation through the nicotinic receptor channel. *PLoS Comput. Biol.* **2008**, *4*, e41.
- (35) Darden, T.; York, D.; Pedersen, L. Particle Mesh Ewald - an NLog(N) Method for Ewald Sums in Large Systems. *J. Chem. Phys.* **1993**, *98*, 10089.
- (36) Tuckerman, M.; Berne, B. J.; Martyna, G. J. Reversible Multiple Time Scale Molecular-Dynamics. *J. Chem. Phys.* **1992**, *97*, 1990.
- (37) Luedtke, R. R.; Freeman, R. A.; Boundy, V. A.; Martin, M. W.; Huang, Y.; Mach, R. H. Characterization of (125)I-IABN, a novel azabicyclonanone benzamide selective for D2-like dopamine receptors. *Synapse* **2000**, *38*, 438.
- (38) Maestro, 5.1; Schrodinger, LLC: New York, 2002.
- (39) ROCS, 2.3.1; OpenEye Scientific Software: Santa Fe, NM, 2007.
- (40) EON, 2.0.1; OpenEye Scientific Software: Santa Fe, NM, 2007.
- (41) Golbraikh, A.; Tropsha, A. Beware of q2! *J. Mol. Graphics Modell.* **2002**, *20*, 269.
- (42) Golbraikh, A.; Shen, M.; Xiao, Z.; Xiao, Y. D.; Lee, K. H.; Tropsha, A. Rational selection of training and test sets for the development of validated QSAR models. *J. Comput.-Aided Mol. Des.* **2003**, *17*, 241.
- (43) Tropsha, A.; Golbraikh, A. Predictive QSAR modeling workflow, model applicability domains, and virtual screening. *Curr. Pharm. Des.* **2007**, *13*, 3494.
- (44) Sachs, L. *Applied Statistics. A Handbook of Techniques.*: Springer-Verlag: New York, 1984; p 349.
- (45) Laskowski, R. A.; MacArthur, M. W.; Moss, D. S.; Thornton, J. M. PROCHECK: A program to check the stereochemical quality of protein structures. *J. Appl. Crystallogr.* **1993**, *26*, 283.
- (46) Ramachandran, G. N.; Ramakrishnan, C.; Sasisekharan, V. Stereochemistry of polypeptide chain configurations. *J. Mol. Biol.* **1963**, *7*, 95.
- (47) Shi, L.; Javitch, J. A. The second extracellular loop of the dopamine D2 receptor lines the binding-site crevice. *Proc. Natl. Acad. Sci. U. S. A.* **2004**, *101*, 440.
- (48) Brady, G. P., Jr.; Stouten, P. F. Fast prediction and visualization of protein binding pockets with PASS. *J. Comput.-Aided Mol. Des.* **2000**, *14*, 383.
- (49) Warne, T.; Serrano-Vega, M. J.; Baker, J. G.; Moukhametianov, R.; Edwards, P. C.; Henderson, R.; Leslie, A. G.; Tate, C. G.; Schertler, G. F. Structure of a betal-1-adrenergic G-protein-coupled receptor. *Nature* **2008**, *454*, 486.
- (50) Kulagowski, J. J.; Broughton, H. B.; Curtis, N. R.; Mawer, I. M.; Ridgill, M. P.; Baker, R.; Emms, F.; Freedman, S. B.; Marwood, R.; Patel, S.; Patel, S.; Ragan, C. I.; Leeson, P. D. 3-((4-(4-Chlorophenyl)piperazin-1-yl)-methyl)-1H-pyrrolo-2,3-b-pyridine: an antagonist with high affinity and selectivity for the human dopamine D4 receptor. *J. Med. Chem.* **1996**, *39*, 1941.
- (51) Simpson, M. M.; Ballesteros, J. A.; Chiappa, V.; Chen, J.; Suehiro, M.; Hartman, D. S.; Godel, T.; Snyder, L. A.; Sakmar, T. P.; Javitch, J. A. Dopamine D4/D2 receptor selectivity is determined by A divergent aromatic microdomain contained within the second, third, and seventh membrane-spanning segments. *Mol. Pharmacol.* **1999**, *56*, 1116.
- (52) Clark, R. D.; Sprous, D. G.; Leonard, J. M. In *Validating models based on large dataset, 13th European Symposium on Quantitative Structure-Activity Relationships 2001*; Holtje, H. D.; Sippel, W., Eds.; Prous Science: Barcelona, Spain, 2001; p 475.
- (53) Neve, K. A.; Cumbay, M. G.; Thompson, K. R.; Yang, R.; Buck, D. C.; Watts, V. J.; DuRand, C. J.; Teeter, M. M. Modeling and mutational analysis of a putative sodium-binding pocket on the dopamine D2 receptor. *Mol. Pharmacol.* **2001**, *60*, 373.
- (54) Lan, H.; Durand, C. J.; Teeter, M. M.; Neve, K. A. Structural determinants of pharmacological specificity between D(1) and D(2) dopamine receptors. *Mol. Pharmacol.* **2006**, *69*, 185.
- (55) Kalani, M. Y.; Vaidehi, N.; Hall, S. E.; Trabanino, R. J.; Freddolino, P. L.; Kalani, M. A.; Floriano, W. B.; Kam, V. W.; Goddard, W. A., III. The predicted 3D structure of the human D2 dopamine receptor and the binding site and binding affinities for agonists and antagonists. *Proc. Natl. Acad. Sci. U. S. A.* **2004**, *101*, 3815.
- (56) Erickson, S. S.; Cummings, D. F.; Weinstein, H.; Schetz, J. A. Ligand selectivity of D2 dopamine receptors is modulated by changes in local dynamics produced by sodium binding. *J. Pharmacol. Exp. Ther.* **2009**, *328*, 40.
- (57) Nilsson, J.; Homan, E. J.; Smilde, A. K.; Grol, C. J.; Wikstrom, H. A multiway 3D QSAR analysis of a series of (S)-N-[(1-ethyl-2-pyrrolidinyl)methyl]-6-methoxybenzamides. *J. Comput.-Aided Mol. Des.* **1998**, *12*, 81.
- (58) Hansch, C.; Verma, R. P.; Kurup, A.; Mekapati, S. B. The role of QSAR in dopamine interactions. *Bioorg. Med. Chem. Lett.* **2005**, *15*, 2149.
- (59) Samanta, S.; Debnath, B.; Gayen, S.; Ghosh, B.; Basu, A.; Srikanth, K.; Jha, T. QSAR modeling on dopamine D2 receptor binding affinity of 6-methoxy benzamides. *Farmaco* **2005**, *60*, 818.